



## OPEN ACCESS

EDITED BY  
Xiaoli Liu,  
Jilin University, China

REVIEWED BY  
Rui Wang,  
First Hospital of Northwest University, China  
Yu Qin,  
Fourth Affiliated Hospital of China Medical  
University, China

\*CORRESPONDENCE  
Ling Chen  
✉ [ling.chen02@fdeent.org](mailto:ling.chen02@fdeent.org)

†These authors have contributed equally to  
this work

RECEIVED 04 May 2025  
ACCEPTED 09 June 2025  
PUBLISHED 30 June 2025

CITATION  
Ma Y, Suo J, Sheng S and Chen L (2025)  
PD-L1 deficiency exacerbates colitis severity  
by remodeling gut microbiota in  
inflammatory bowel disease.  
*Front. Immunol.* 16:1622744.  
doi: 10.3389/fimmu.2025.1622744

COPYRIGHT  
© 2025 Ma, Suo, Sheng and Chen. This is an  
open-access article distributed under the terms  
of the [Creative Commons Attribution License  
\(CC BY\)](https://creativecommons.org/licenses/by/4.0/). The use, distribution or reproduction  
in other forums is permitted, provided the  
original author(s) and the copyright owner(s)  
are credited and that the original publication  
in this journal is cited, in accordance with  
accepted academic practice. No use,  
distribution or reproduction is permitted  
which does not comply with these terms.

# PD-L1 deficiency exacerbates colitis severity by remodeling gut microbiota in inflammatory bowel disease

Yixian Ma<sup>1,2,3†</sup>, Jinshan Suo<sup>4†</sup>, Siqi Sheng<sup>1,2,3</sup> and Ling Chen<sup>1,2,3,5\*</sup>

<sup>1</sup>Eye Institute and Department of Ophthalmology, Eye & ENT Hospital, Fudan University, Shanghai, China, <sup>2</sup>Shanghai Key Laboratory of Visual Impairment and Restoration, Shanghai, China, <sup>3</sup>NHC Key Laboratory of Myopia and Related Eye Diseases, Key Laboratory of Myopia and Related Eye Diseases, Chinese Academy of Medical Sciences, Shanghai, China, <sup>4</sup>Department of Immunology, School of Cell and Gene Therapy, Songjiang Research Institute, Shanghai Songjiang District Central Hospital, Shanghai Jiao Tong University School of Medicine, Shanghai, China, <sup>5</sup>Ophthalmology Medical Center, The First Affiliated Hospital of Chongqing Medical University, Chongqing Key Laboratory for the Prevention and Treatment of Major Blinding Eye Diseases, Chongqing Branch (Municipality Division) of National Clinical Research Centre for Ocular Diseases, Chongqing, China

**Background:** Inflammatory bowel disease (IBD) is a chronic autoimmune disorder driven by gut microbiota dysbiosis. As an essential immune checkpoint, Programmed death-ligand 1 (PD-L1) has been implicated in modulating gut microbiota composition. However, the precise role of PD-L1 in shaping metagenomic profiles during IBD-associated colitis remains unexplored.

**Methods:** DSS-induced colitis was established in both PD-L1 knockout (*Pdcd1lg1*<sup>-/-</sup>) mice and wild-type (wt) control mice. Clinical parameters, including disease activity index (DAI), body weight changes, colon length, and histopathological alterations, were systematically evaluated using non-parametric Kruskal-Wallis tests and ANOVA to compare colitis severity between genotypes.

**Results:** PD-L1 knockout mice exhibited exacerbated colitis, manifesting significantly greater weight loss ( $p < 0.05$  vs. wt\_DSS), colonic shortening ( $p < 0.05$ ), and DAI scores ( $p < 0.05$ ) and inflammatory changes. PD-L1 knockout mice showed distinct dysbiosis, with enriched pathobionts (*Escherichia coli*,  $p = 0.006$ ; *Bacteroides thetaiotaomicron*,  $p = 0.015$ ) and depletion of commensals (*Trichomonas foetus*,  $p < 0.001$ ; *Ligilactobacillus murinus*). Alpha diversity analysis using Chao1 index revealed statistically significant differences between experimental groups ( $p = 0.05$ ). The transporters downregulate anti-inflammatory SCFA metabolism. KEGG enrichment analysis of differentially expressed genes (DEGs) revealed significant associations with immune and inflammatory pathways in PD-L1 knockout mice.

**Conclusion:** PD-L1 deficiency aggravates colitis by driving pathogenic microbiota alterations and impairing microbial metabolic homeostasis, highlighting its dual regulatory roles in immune homeostasis and microbiome dynamics.

## KEYWORDS

programmed death ligand 1 (PD-L1), gut microbiota, metagenomic analysis, autoimmunity, inflammatory bowel disease (IBD)

## 1 Introduction

Inflammatory bowel disease (IBD), encompassing Crohn's disease (CD) and ulcerative colitis (UC), is a chronic and relapsing inflammatory disorder of the gastrointestinal tract with rising global incidence, particularly in industrialized nations (1, 2). IBD is more common in young and middle-aged adults, but the incidence has been increasing in children and the elderly in recent years. Some studies show that the male-to-female ratio for UC is nearly equal, while CD is slightly more prevalent in females (2, 3).

Environmental triggers such as dietary patterns, pharmacological exposures, and lifestyle factors significantly impact gut microbiota homeostasis. Excessive consumption of high-fat/low-fiber diets and inappropriate antibiotic use have been shown to disrupt microbial symbiosis, resulting in diminished production of beneficial metabolites including short-chain fatty acids (SCFAs) while simultaneously impairing intestinal epithelial barrier integrity (4, 5). Epidemiological studies highlight that the prevalence of IBD exhibits notable geographical variations. For example, gut microbiota profiles of patients from Mexico and Spain differ significantly due to dietary differences, and microbiome characteristics in Middle Eastern populations may influence IBD risk through specific dietary patterns, such as high-fiber and fermented foods consumption (6, 7).

The pathogenesis of IBD involves complex multifactorial interactions, primarily including genetic susceptibility, mutations in specific genes (e.g., NOD2, IL23R) increase the risk of intestinal barrier defects or aberrant immune responses (1, 2). Immune dysregulation in IBD involves aberrant immune responses against gut microbiota, characterized by excessive production of pro-inflammatory cytokines such as TNF- $\alpha$ , IL-6, and IL-17, coupled with insufficient anti-inflammatory mediators including IL-10 (8–10). Intestinal barrier disruption primarily arises from impaired epithelial tight junction complexes, particularly involving occludin and claudin proteins, which compromise mucosal integrity and facilitate microbial translocation, thereby triggering innate immune activation through the leaky gut mechanism (10, 11).

Notably, the gut microbiota has emerged as a pivotal contributor, where dysbiosis—characterized by reduced microbial diversity, depletion of commensal bacteria (e.g., *Faecalibacterium prausnitzii*), and expansion of pathobionts (e.g., *Escherichia coli*)—disrupts mucosal homeostasis and drives aberrant immune activation (12, 13). Altered microbial metabolites (e.g., secondary bile acids, hydrogen sulfide) disrupt redox homeostasis and potentiate pro-inflammatory responses via oxidative stress-mediated pathways (7, 14).

The programmed death-ligand 1 (PD-L1), encoded by the gene *Pdcd1lg1*, is a critical immune checkpoint protein that interacts with programmed death-1 (PD-1) on T cells. This interaction inhibits T cell activation and proliferation, thereby preventing excessive immune responses. It also promotes the differentiation of regulatory T cells (Tregs) and induces effector T-cell exhaustion, maintaining immune tolerance. Additionally, it modulates inflammatory cytokines such as IFN- $\gamma$  and IL-2 (15, 16). In the intestinal microenvironment, PD-L1 exhibits context-dependent

functions. The gut microbiota composition directly modulates PD-1/PD-L1 inhibitor efficacy, where specific probiotics, such as *Bifidobacterium*, enhance anti-PD-1 therapeutic response through PD-L2 downregulation (17). Studies demonstrate that intestinal epithelial cells upregulate PD-L1 following stimulation with gut microbial metabolites (e.g., L-DNA), promoting activated Th2 cell apoptosis to modulate local intestinal immune responses (18). PD-L1 deficiency disrupts gut microbiota homeostasis and exacerbates DSS-induced colitis (19). In contrast, PD-L1 attenuates intestinal graft injury through innate immune response suppression during intestinal transplantation, demonstrating its essential role in preserving intestinal immune homeostasis (20, 21).

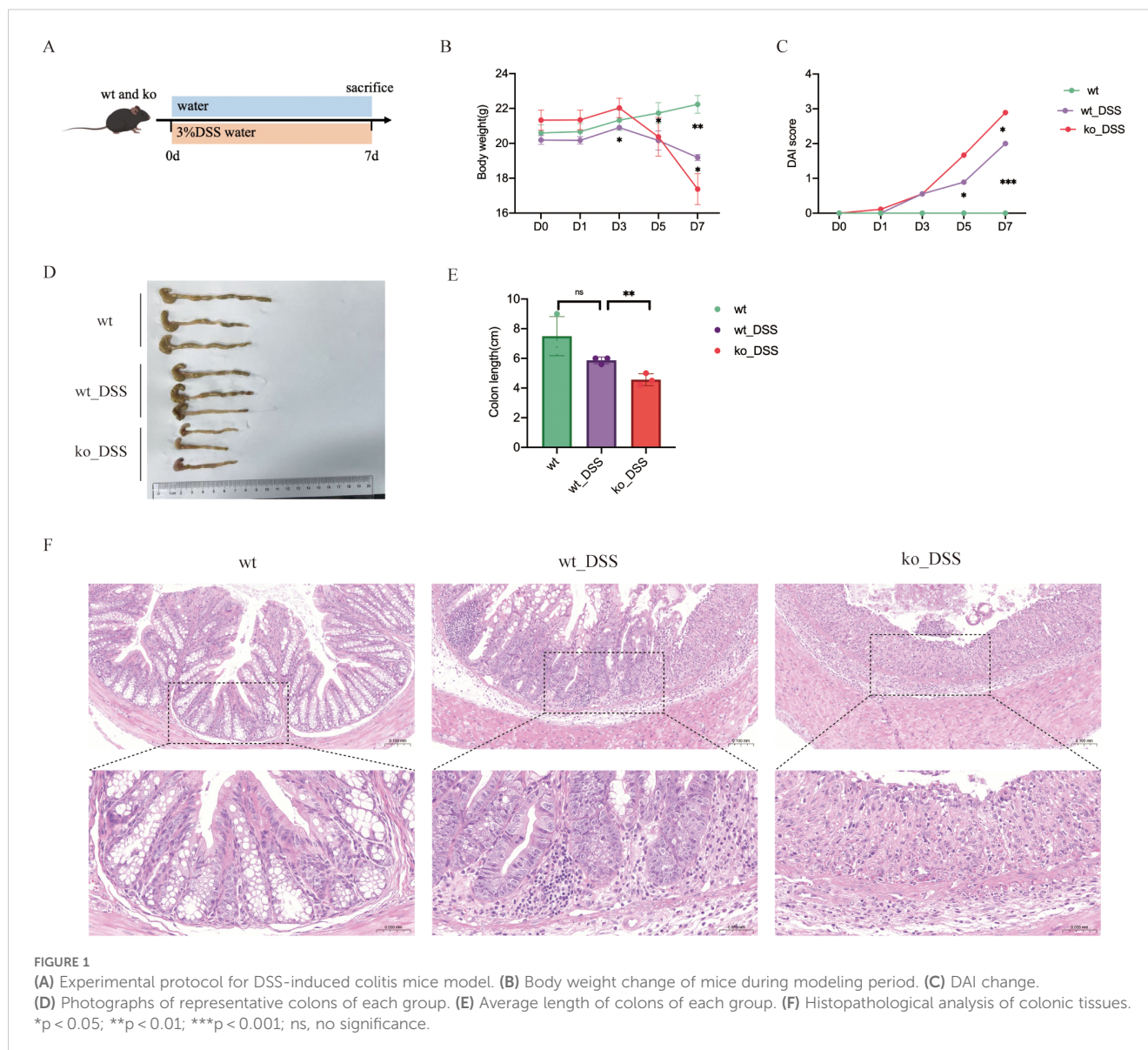
Although studies on gut microbiota in IBD and the association between PD-L1 and microbiota are increasing, systematic investigations into the gut microbiota in PD-L1 deficiency-mediated colitis remain insufficient. This study aims to explore the impact of *Pdcd1lg1* knockout on gut microbiota composition in C57BL/6J mice under inflammatory bowel disease conditions. It systematically investigates the effects of PD-L1 genetic ablation on gut microbiota composition in C57BL/6J mice under experimental colitis conditions.

## 2 Materials and methods

### 2.1 Animals and experimental design

Female C57BL/6J mice and female *Pdcd1lg1* knockout C57BL/6J mice (*Pdcd1lg1*  $-/-$  mice), aged 6–8 weeks, were obtained from Cyagen Biosciences, Suzhou, China. All experimental procedures were performed according to the guidelines of the Animal Care and Use Committee of Fudan University (Shanghai, China). Animals were housed at the Experimental Animal Center of the Eye and ENT Hospital of Fudan University with a temperature of 22–26°C, 12-hour light/dark cycles, and relative humidity of 40–70%.

Then, animals were randomly divided into four groups (n=3/group) including wt\_control (wild-type without DSS), ko\_control (*Pdcd1lg1*  $-/-$  without DSS), wt\_DSS (wild-type with DSS-induced colitis), and ko\_DSS (*Pdcd1lg1*  $-/-$  with DSS-induced colitis) (Dextran Sulfate Sodium, Yeasen biotech Co., Ltd., Shanghai, China). Colitis was induced in mice by daily administration of 3% DSS for 7 days, while the control group received equivalent volumes of sterile distilled water (Figure 1A). Body weights were recorded at baseline (day 0) and on day 1, 3, 5, and 7 post-modeling. On day 7, mice were sacrificed via cervical dislocation under anesthesia (1.25% bromethol, 0.2 mL/10g body weight administered intraperitoneally; Aibei Biotechnology Co., Ltd., Nanjing, China). Collect fecal specimens and obtain colonic samples extending from the cecum junction to the anal verge. Immediately after collection, the fecal specimens were flash-frozen in liquid nitrogen and then stored at -80°C to maintain microbial viability and DNA integrity for subsequent sequencing analysis. Colon length was measured along the mesenteric border before fixation in 4% paraformaldehyde, followed by paraffin embedding and hematoxylin & eosin (H&E) staining. The disease



activity index (DAI) was calculated to assess the severity of UC in animal models in light of the study (22).  $DAI = (\text{Weight loss score} + \text{Stool score} + \text{Bleeding score})/3$ .

## 2.2 Metagenome DNA extraction and shotgun sequencing

Total microbial genomic DNA was extracted from fecal samples using the OMEGA Mag-Bind Soil DNA Kit (M5635-02; Omega Bio-Tek, GA, USA) according to the manufacturer's protocol, and stored at  $-20^{\circ}\text{C}$  until further assessment. DNA concentration and purity were quantified using a Qubit<sup>TM</sup> 4 Fluorometer (Thermo Fisher Scientific Inc., MA, USA), while integrity was verified by agarose gel electrophoresis. The extracted microbial DNA was processed to construct metagenome shotgun sequencing libraries with insert sizes of  $\sim 400$  bp by using Illumina TruSeq Nano DNA LT Library Preparation Kit (Illumina, CA, USA). Each library was sequenced

by Illumina NovaSeq platform (Illumina, CA, USA) with PE150 strategy at Personal Biotechnology Co., Ltd. (Shanghai, China).

## 2.3 Metagenomics analysis

Raw sequencing reads were processed through adapter removal with Cutadapt (v1.2.1) (23), sliding-window quality trimming using fastp (v0.23.2) (24), and host DNA removal by alignment to the mouse genome via Minimap2 (v2.24-r1122) to generate quality-filtered data (25). Once quality-filtered reads were obtained, taxonomical classifications of metagenomics sequencing reads from each sample were performed using Kraken2 (v2.0.8 beta) (26) against databases including NCBI-nt, GTDB and RVDB. Reads assigned to metazoans or viridiplantae were removed for downstream analysis. Megahit (v1.1.2) (27) was used for assembly of reads in each sample using the meta-large preset parameters. The generated contigs (longer than 300bp) were then pooled

together and clustered using MMseqs2 (version 13.45111) (28) with “easy-linclud” mode, setting sequence identity threshold to 0.95 and covered residues of the shorter contig to 90%. The lowest common ancestor taxonomy of the non-redundant contigs was obtained by aligning them against the NCBI-nt database by MMseqs2 with “taxonomy” mode, and contigs assigned to Viridiplantae or Metazoa were dropped in the following analysis. Prodigal (V2.6.3) (29) was used to predict the genes in the contigs. CDS sequences of all samples were clustered by MMseqs2 with “easy-cluster” mode, setting protein sequence identity threshold to 0.95 and covered residues of the shorter contig to 90%. To assess the abundances of these genes, the high-quality reads from each sample were mapped onto the predicted gene sequences using Minimap2 with “-ax sr -sam-hit-only” and using featureCounts to count the number of reads aligned to gene sequences, i.e., the Reads Count (RC) (30) for each gene. The functionality of the non-redundant genes was obtained by annotated using MMseqs2 with the “search” mode against the protein databases of KEGG.

## 2.4 Statistical analyses

In this study, statistical tests (Kruskal-Wallis test, ANOVA) were conducted using R software (version 3.6.1). Based on the taxonomic and functional profiles of non-redundant genes, LEfSe (Linear discriminant analysis effect size) was performed to detect differentially abundant taxa and functions across groups using the default parameters (31). Beta diversity analysis was performed to investigate the compositional and functional variation of microbial communities across samples using Bray-Curtis distance metrics (32) and visualized via principal coordinate analysis (PCoA), nonmetric multidimensional scaling (NMDS) and unweighted pair-group method with arithmetic means (UPGMA) hierarchical clustering (33).  $P < 0.05$ ,  $P < 0.01$  and  $P < 0.001$  were considered significant. GraphPad Prism 9.0 software (GraphPad Software Inc, La Jolla, CA, USA) was used to draw images.

## 3 Results

### 3.1 PD-L1 knockout mice had more severe intestinal inflammation

All mice exhibited normal activity, dietary intake, stool consistency, and weight gain before modelling. In comparison with those in the control group, the mice in the model group showed not only significantly decreased body weight (Figure 1B) and colon length (Figures 1D, E), but also observably increased DAI scores (Figure 1C). Both wt\_DSS and ko\_DSS groups experienced significant weight loss compared to their respective controls ( $p < 0.05$ ). Notably, the ko\_DSS group showed more pronounced weight loss than the wt\_DSS group ( $p < 0.05$ ), indicating exacerbated colitis in *Pdcd1lg1*  $-/-$  mice (Figure 1B). The wt\_DSS group had shorter colons than the wt control ( $p < 0.05$ ), reflecting colitis-induced shortening. The ko\_DSS group exhibited the shortest

colons ( $p < 0.05$  vs. wt\_DSS), suggesting more severe colitis in *Pdcd1lg1*  $-/-$  mice (Figures 1D, E). Both wt\_DSS and ko\_DSS groups had higher DAI scores than wt group ( $p < 0.05$ ). The ko\_DSS group had the highest DAI scores ( $p < 0.05$  vs. wt\_DSS), indicating the most severe colitis. In addition, the macroscopic morphology of colonic tissues showed colon edema, a reduced caecal volume and an enteric cavity with bloody stools. The ko\_DSS group mice exhibited severed colonic shortening and colonic edema than both wt group mice and wt\_DSS group mice (Figure 1F).

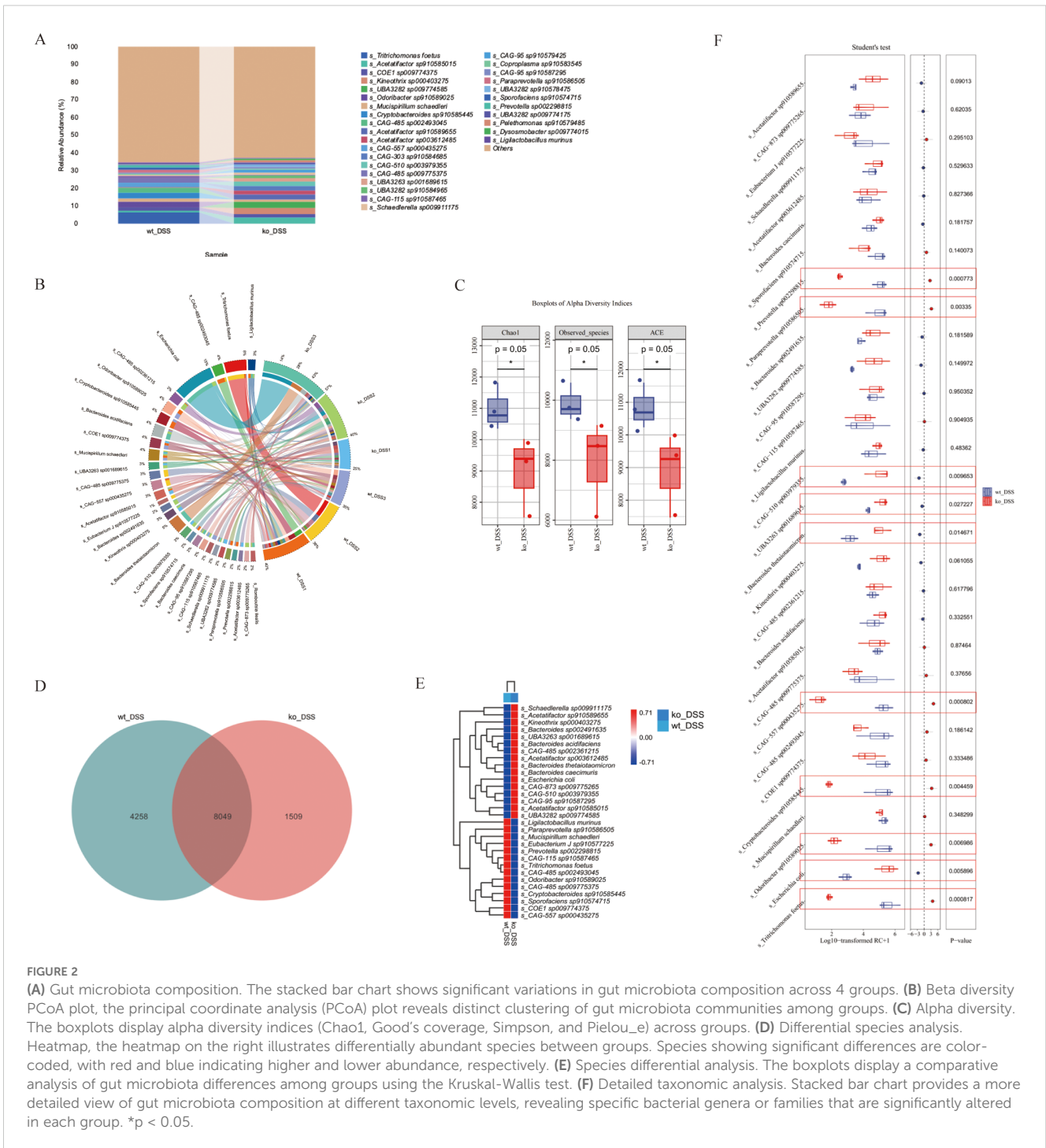
### 3.2 The gut microbiota in four groups is altered

We performed metagenomic sequencing on fecal samples from four groups of mice: wt, wt\_DSS, ko, and ko\_DSS. Our analysis revealed distinct gut microbiota compositions among the groups. We focused on microbes with an abundance of 30. In the colitis model groups (wt\_DSS and ko\_DSS), the gut microbiota shifted notably. Specifically, *Escherichia coli* and *Bacteroides* increased significantly in the ko\_DSS group, while *Tritrichomonas* was more abundant in the wt\_DSS group. In the control groups, the gut microbiota also differed between the wt and ko groups. The ko group had higher abundances of *Limosilactobacillus* and CAG-485 sp002361215, whereas the wt group showed higher levels of *Dubosiella*, *Akkermansia*, and CAG-485 sp002491945 (Figure 2A). A PCoA plot (Figure 2B) and a clustering heatmap (Figure 2C) both highlighted the distinct compositional differences between groups. Alpha diversity analysis (Figure 2D) indicated no significant differences in some indices, but notable changes in others, such as the trend in Chao1 diversity. Species differential analysis revealed that *Escherichia* levels varied significantly across groups ( $p < 0.05$ ). While *Odoribacter* sp910589025, *Limosilactobacillus reuteri*, *Akkermansia muciniphila* A, *Ligilactobacillus murinus*, and *Tritrichomonas foetus* did not show statistical differences, their abundances changed markedly (Figure 2E). Finally, LEfSe analysis identified differentially abundant gut microbial taxa at various taxonomic levels, pinpointing specific bacterial genera or families that changed significantly in each group (Figure 2F).

This study primarily examines the alterations in gut microbiota composition between the wt\_DSS and ko\_DSS groups.

### 3.3 PD-L1 modulates gut microbiota composition in DSS-induced colitis mice

Evaluation of gut microbiota in the DSS-induced colitis model revealed alterations in both the wt\_DSS and ko\_DSS groups (Figures 3A, B). The two groups shared 8,049 bacterial genera, while the wt\_DSS and ko\_DSS groups exhibited 1,509 and 4,258 unique genera, respectively (Figure 3D). Alpha diversity indices were used to assess the gut microbiota, showing significant differences in richness (Chao1, Observed species, and ACE) between the two groups ( $p = 0.05$ ). However, no significant differences were observed in diversity (Simpson index), evenness



(Pielou's evenness), or coverage (Good's coverage) (Figure 3C). The wt\_DSS group showed higher enrichment of *Schaedlerella* sp009911175, *Acetatifactor* sp910589655, *Kineothrix* sp000403275, *Bacteroides* sp00249163, *UBA3263* sp001689615, *Bacteroides acidifaciens*, *CAG-485* sp002361215, *Acetatifactor* sp003612485, *Bacteroides thetaiotaomicron*, *Bacteroides caecimuris*, *Escherichia coli*, *CAG-873* sp009775265, *CAG-510* sp003979355, *CAG-95* sp910587295, *Acetatifactor* sp910585015, and *UBA3282* sp009774585. In contrast, *Ligilactobacillus murinus*, *Paraprevotella* sp910586505, *Mucispirillum schaedleri*, *Eubacterium J* sp910577225,

*Prevotella* sp002298815, *CAG-115* sp910587465, *Tritrichomonas foetus*, *CAG-485* sp002493045, *Odoribacter* sp910589025, *CAG-485* sp009775375, *Cryptobacteroides* sp910585445, *Sporofaciens* sp910574715, *COE1* sp009774375, and *CAG-557* sp000435275 were less enriched. The ko\_DSS group exhibited the opposite trend (Figure 3E). Further differential species analysis identified significantly higher enrichment of *Escherichia coli* ( $p = 0.0058$ ), *CAG-510* sp003979355 ( $p = 0.010$ ), *UBA3263* sp001689615 ( $p = 0.027$ ), and *Bacteroides thetaiotaomicron* ( $p = 0.015$ ). Conversely, *Tritrichomonas foetus* ( $p < 0.001$ ), *CAG-557* sp000435275 ( $p <$

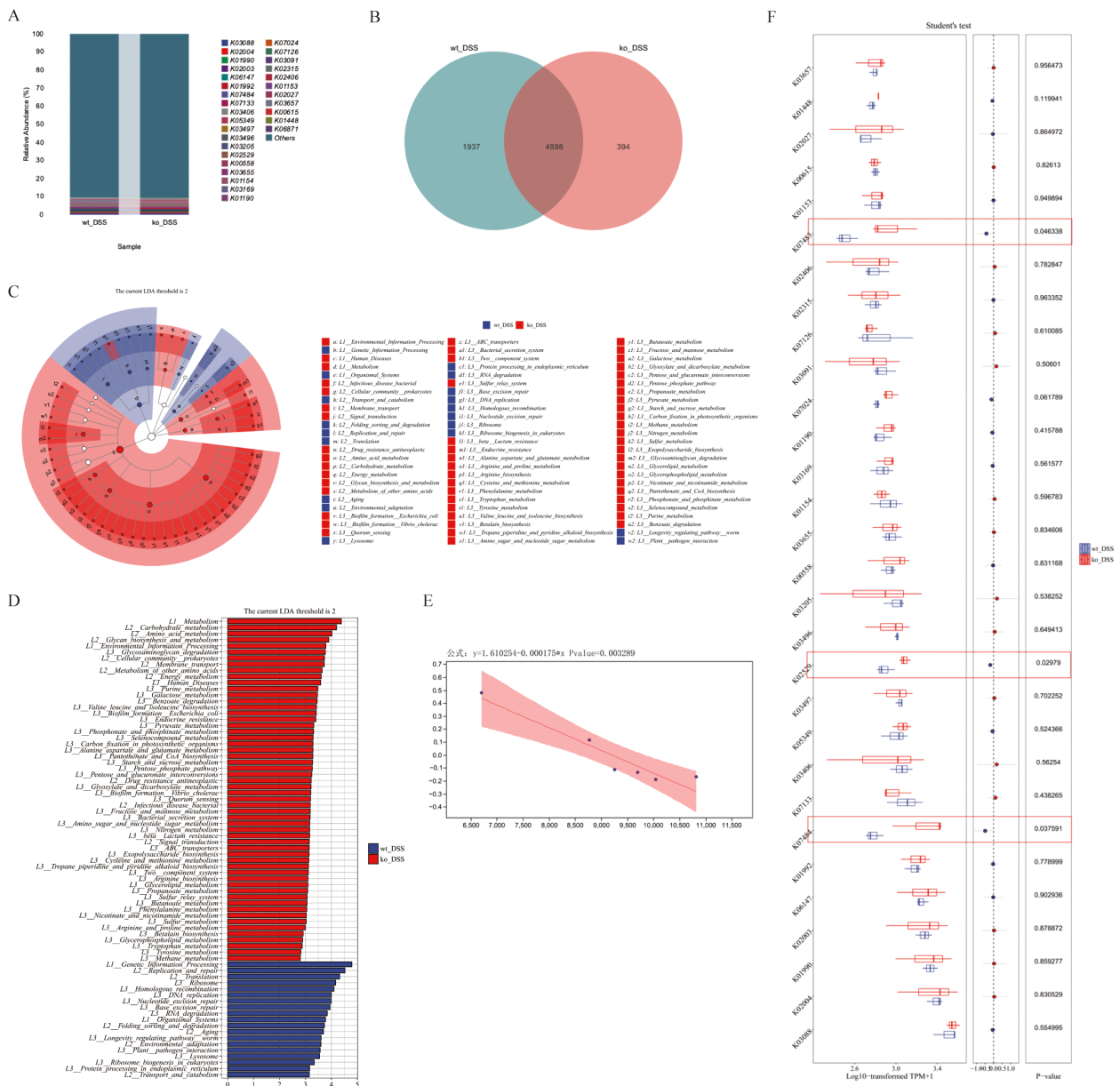


**FIGURE 3**  
**(A)** Gut microbiota composition. The stacked bar chart shows the relative abundance of gut microbiota compositions between ko\_DSS and wt\_DSS groups. X-axis: Group names; Y-axis: Relative abundance of KEGG species levels. **(B)** Species differential analysis. This Circos Plot illustrates differentially abundant species between the two groups. Left: Abundance values (top 30); Right: Sample names. Colors in the inner ring mark species, and the outer ring shows their abundance. **(C)** Alpha diversity analysis. Boxplots indices (Chao1, Observed\_species, ACE) across groups. Each panel corresponds to an alpha diversity index, as indicated in the grey area at the top. In each panel, the x-axis represents the group labels, and the y-axis represents the value of the corresponding alpha diversity index. In the boxplot, the elements are defined as follows: the top and bottom lines of the box represent the upper and lower quartiles (Interquartile Range, IQR); the central line denotes the median; the upper and lower whiskers indicate the maximum and minimum values (extremes within 1.5 times the IQR range); and points outside the whiskers represent outliers. The Kruskal-Wallis test was used to assess diversity indices, followed by Dunn's test for *post hoc* analysis. A p-value less than 0.05 indicates statistically significant differences. **(D)** The composition Venn. The Venn diagram shows shared and unique species between ko\_DSS and wt\_DSS groups. Each colored block represents a group. Overlapping areas indicate shared species between groups, with numbers denoting species counts per region. **(E)** The composition heatmap. The groups are first clustered based on the similarity of their species abundance distribution, and then arranged horizontally according to the clustering results. Similarly, taxonomic units are clustered based on their distribution similarity across different groups and arranged vertically based on the clustering outcome. Red (0.71): High relative abundance in a group. White (0.00): Neutral/no significant abundance. Blue (-0.71): Low relative abundance or depletion. **(F)** The Boxplots Diagram. The diagram shows the species-level differential abundance analysis (normalized). Student's t-test was applied for pairwise comparisons, with significant p-values marked. Red circles denote genes with statistically significant functional differences. DSS, Dextran sulphate sodium; ko, knockout; wt, wild-type.

0.001), *Paraprevotella* sp910586505 ( $p = 0.003$ ), *Cryptobacteroides* sp910585445 ( $p = 0.0044$ ), *Odoribacter* sp910589025 ( $p = 0.0069$ ), and *Prevotella* sp002298815 ( $p = 0.008$ ) were significantly less enriched (Figure 3F).

### 3.4 PD-L1 alters gut microbiota functional units in DSS-induced colitis mice

We next performed functional analysis of the gut microbiota in colitis model groups. The intergroup differences in microbial composition significantly altered gene functional profiles. Statistical analysis of feature tables using the KEGG database enabled visualization of compositional distribution at functional classification levels (top 30 categories), presented as a bar chart (Figure 4A). Comparative analysis revealed 4,898 shared functional genes between groups, with 394 and 1,937 genes uniquely identified in the ko\_DSS and wt\_DSS groups, respectively (Figure 4B). Subsequently, LEfSe (LDA Effect Size) analysis was employed to rank differentially enriched functional pathways between ko\_DSS and wt\_DSS groups. Results demonstrated that the ko\_DSS group exhibited significant enrichment of pathways associated with pro-inflammatory and pathogenic functions, including: Bacterial secretion systems (Type III/IV), linked to virulence traits in *Escherichia coli* and *CAG taxa*. ABC transporters (e.g., K02003/K02004) and drug resistance pathways, suggesting enhanced antibiotic resistance in ko\_DSS. Immune dysregulation-related pathways, such as the lysosome pathway (associated with heightened phagocytic activity due to inflammation) and detoxification/detoxification (reflecting oxidative stress in chronic colitis). In contrast, the wt\_DSS group showed enrichment of pathways supporting anti-inflammatory and metabolic homeostasis, including: Short-chain fatty acid (SCFA) metabolism (e.g., butyrate synthesis via K01990), which promotes Treg differentiation and epithelial barrier integrity. Carbohydrate metabolism (e.g., glycosyl hydrolases), driven by dietary fiber fermentation from *Ligilactobacillus* and *Bacteroides*. Ribosome biosynthesis, indicative of stable microbiome-protein synthesis. Commensal-mucosal crosstalk pathways (e.g., arginine/proline metabolism) modulating nitric oxide (NO) production and immune signaling (Figures 4C, D). Further normalization of functional unit abundances revealed statistically significant enrichment of pro-inflammatory/virulence-associated genes in ko\_DSS (e.g., K07133 [Type III secretion system,  $p = 0.038$ ], K02529 [uncharacterized protein,  $p = 0.030$ ], and K01190 [glycoside hydrolase,  $p = 0.046$ ]). The wt\_DSS group harbored higher abundances of anti-inflammatory/commensal genes (e.g., K01990 [acetyl-CoA synthetase] and K01153 [glycosyl hydrolase]), though these lacked statistical significance (Figure 4F). Finally, linear regression analysis of functional and taxonomic correlations identified a significant negative association ( $p = 0.003$ ) between an immune variable ( $x$ ; e.g., inflammatory cytokine levels) and microbial/metabolic responses ( $y$ ; e.g., beneficial taxon abundance), underscoring PD-L1's role in microbiota-immune crosstalk during colitis (Figure 4E).

### 3.5 PD-L1 regulates gut microbiota genes profiles in DSS-induced colitis mice

Finally, we performed gene-level differential analysis of fecal samples from the mouse model. Compared to the wt\_DSS group, ko\_DSS group exhibited 222,335 genes upregulated and 59,504 genes downregulated genes (Figure 5A). KEGG enrichment analysis of these differentially expressed genes (DEGs) revealed significant associations with immune/inflammatory pathways in ko\_DSS, including: IL-17 signaling, Lipopolysaccharide biosynthesis, Endocrine resistance. Additionally, infection/disease-related pathways were enriched, such as COVID-19, HIV infection and Salmonella infection. Notably, metabolic and cellular dysregulation pathways, including thermogenesis and lysosome, were also altered (Figures 5B, C), suggesting shifts in response to DSS-induced inflammation in *Pcd1lg1* deficient mice.

## 4 Discussion

The study provides compelling evidence that PD-L1 deficiency exacerbates DSS-induced colitis through profound alterations in gut microbiota composition and function. PD-L1 knockout mice exhibited more severe clinical symptoms, such as marked weight loss, colon shortening, and elevated DAI scores, which were accompanied by distinct changes in the microbial community. These changes were characterized by an increase in pathogenic taxa, including *Escherichia coli* and *CAG-510*, and a decrease in beneficial species, such as *Tritrichomonas foetus* and *Ligilactobacillus murinus*. Notably, metagenomic analysis revealed PD-L1-dependent shifts in microbial virulence pathways and metabolic functions. These findings align with emerging understanding of PD-1/PD-L1 axis in mucosal immunity, while revealing novel microbiota-mediated mechanisms.

The PD-1/PD-L1 pathway is regarded as a potential therapeutic target in IBD. Studies reveal that PD-1 and PD-L1 expression is significantly upregulated in inflamed intestinal mucosa, primarily localized to non-ulcerated regions. This spatial heterogeneity suggests that PD-1/PD-L1 may protect the mucosal barrier by suppressing localized hyperimmune responses, while their loss in ulcerated zones could contribute to uncontrolled inflammation (34). Meanwhile, PD-L1 maintains intestinal homeostasis by modulating dendritic cells (e.g., XCR1+ DCs) and Tregs (35). Since this study primarily focuses on analyzing the impact of gut microbiota changes on colitis, we observed that the PD-L1 knockout mice showed marked depletion of mucin-protective species (*Akkermansia muciniphila*) and SCFA-producers (*L. murinus*), while harboring increased mucolytic bacteria (*Bacteroides thetaiotaomicron*). The observed imbalances likely impair epithelial integrity, as demonstrated by histopathological evidence of severe edema and ulceration, accompanied by downregulation of tight junction genes (including occludin and claudins) and upregulation of bacterial invasion pathways such as the Type III secretion system. Together, these pathological changes collectively disrupt intestinal barrier function.

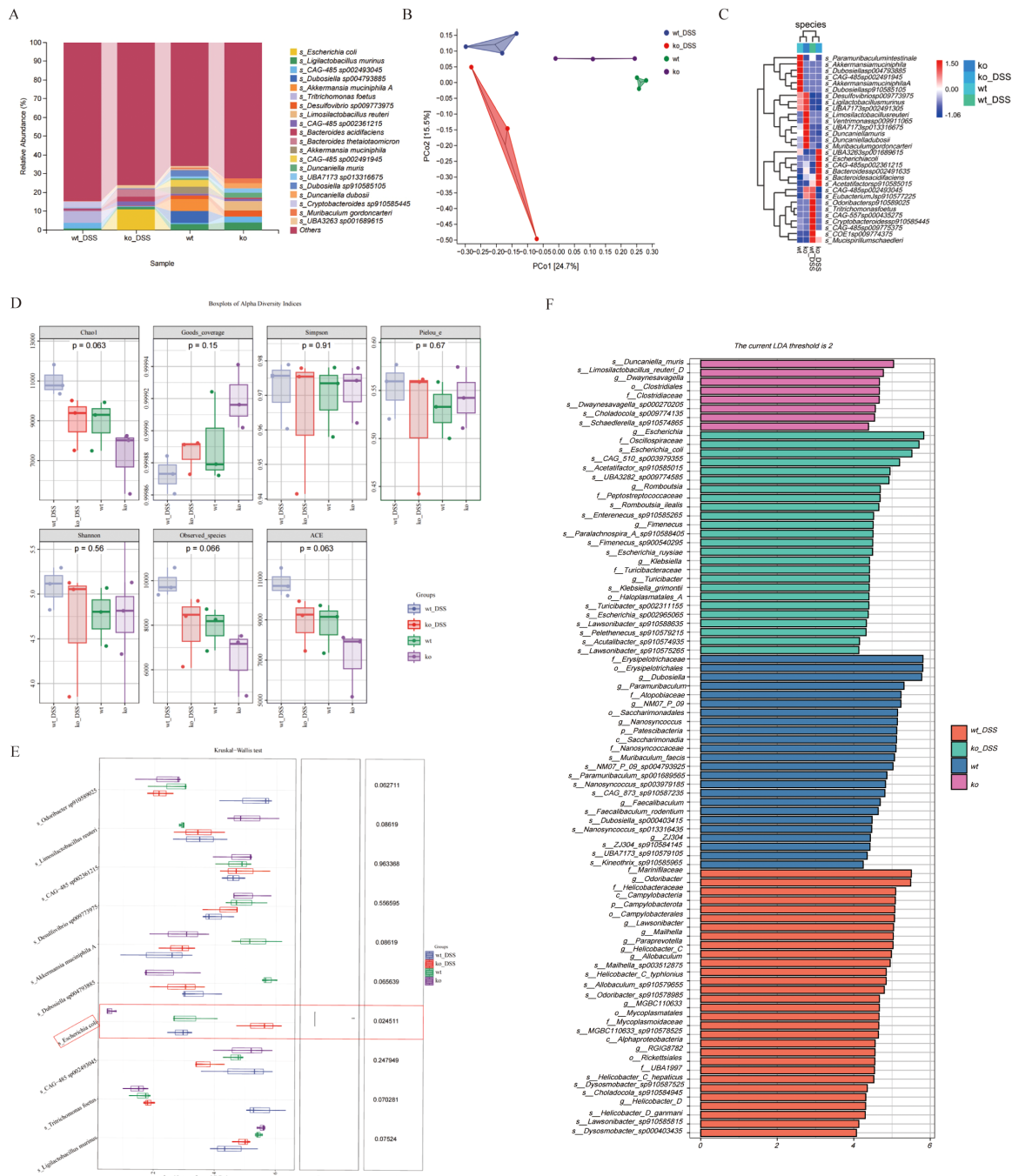


**FIGURE 4**  
**(A)** Gut microbiota functional composition. The stacked bar chart shows the relative abundance of gut microbiota functional compositions between ko\_DSS and wt\_DSS groups. X-axis: Group names; Y-axis: Relative abundance of KEGG functional categories. Rows: KEGG Orthology (KO) identifiers representing microbial metabolic/enzymatic functions. Columns: groups (wt\_DSS and ko\_DSS). Values: Relative abundance (%) of each functional gene category. "Others": Aggregated low-abundance functions. **(B)** The functional Venn. The Venn diagram shows shared and unique species between ko\_DSS and wt\_DSS groups. Each colored block represents a group. Overlapping areas indicate shared functional units between groups, with numbers denoting functional unit counts per region. **(C)** The Circular branching Diagram. Cladogram of LefSe-identified functional pathways in ko\_DSS (red) and wt\_DSS (green) mice. Node size reflects LDA effect size (threshold > 2). Key pathways are annotated (see Results). **(D)** The bar plot displays the functional units with statistically significant differences between ko\_DSS and wt\_DSS groups, as determined by Linear Discriminant Analysis (LDA) effect size (LEfSe). Y-axis: Functional units showing significant intergroup differences ( $p < 0.05$ ). X-axis: LDA score (log<sub>10</sub>-transformed), representing the magnitude of differential abundance. Longer bars indicate stronger discriminatory power. Red: Functional units enriched in ko\_DSS. Green: Functional units enriched in wt\_DSS. **(E)** Linear Regression Plot. This plot shows the relationship between two variables, with a fitted regression line and a shaded confidence interval. The equation and p-value indicate the strength and significance of the relationship. **(F)** The Boxplots Diagram. The diagram shows the statistical comparison of functional gene expression (KEGG Orthology, KO terms) between ko\_DSS and wt\_DSS groups. KO Terms: Listed rows represent microbial metabolic/pathway genes. Expression Values: Log<sub>10</sub>-transformed TPM+1 (Transcripts Per Million, normalized and log-transformed). Student's t-test p-values for each KO term. Group name: wt\_DSS vs. ko\_DSS. Red circles denote genes with statistically significant functional differences. DSS, Dextran sulfate sodium; ko, knockout; wt, wild-type.

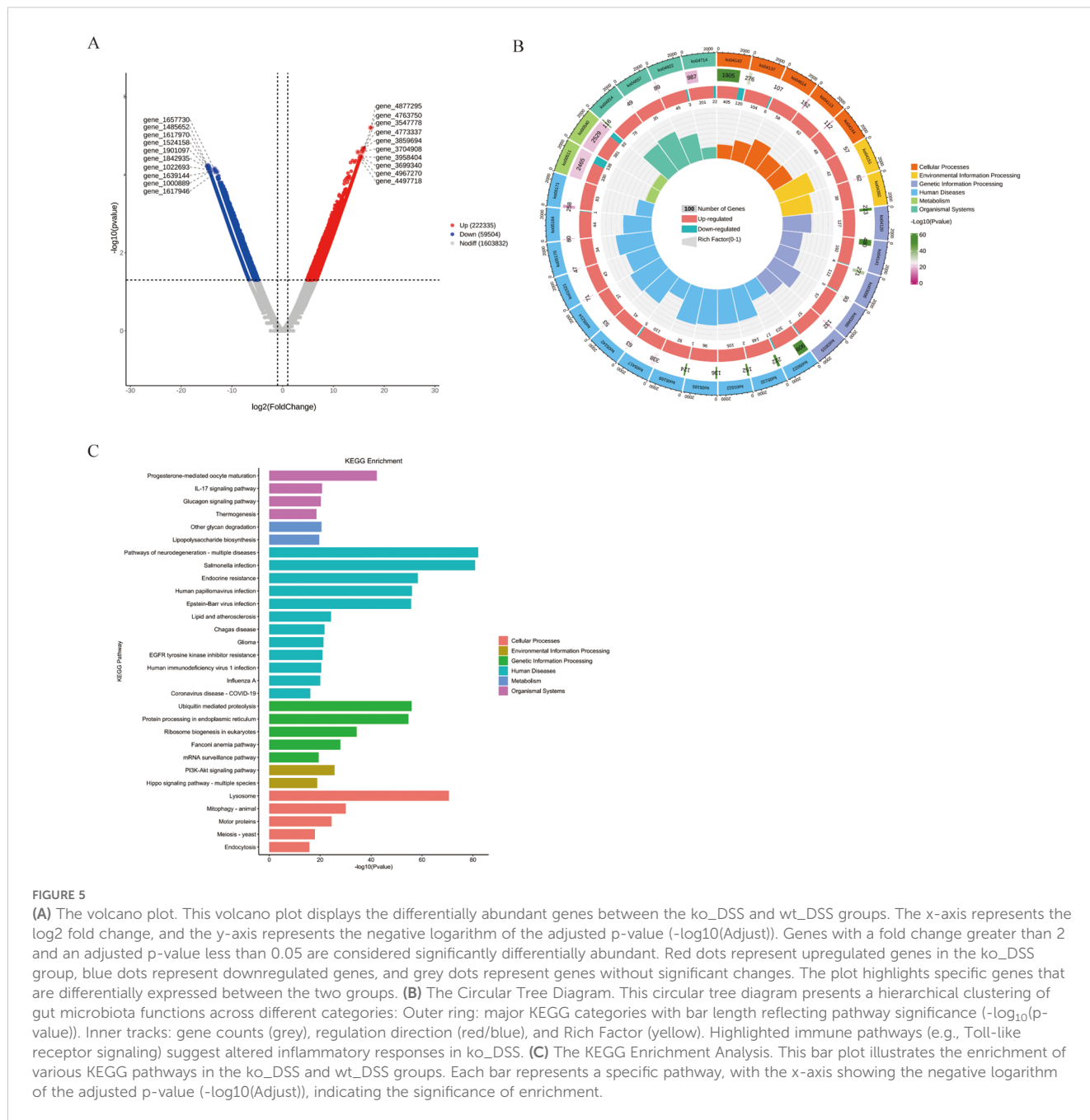


FIGURE 5

(A) The volcano plot displays the differentially abundant genes between the ko\_DSS and wt\_DSS groups. The x-axis represents the  $\log_2$  fold change, and the y-axis represents the negative logarithm of the adjusted p-value ( $-\log_{10}(\text{Adjusted})$ ). Genes with a fold change greater than 2 and an adjusted p-value less than 0.05 are considered significantly differentially abundant. Red dots represent upregulated genes in the ko\_DSS group, blue dots represent downregulated genes, and grey dots represent genes without significant changes. The plot highlights specific genes that are differentially expressed between the two groups. (B) The Circular Tree Diagram. This circular tree diagram presents a hierarchical clustering of gut microbiota functions across different categories: Outer ring: major KEGG categories with bar length reflecting pathway significance ( $-\log_{10}(p\text{-value})$ ). Inner tracks: gene counts (grey), regulation direction (red/blue), and Rich Factor (yellow). Highlighted immune pathways (e.g., Toll-like receptor signaling) suggest altered inflammatory responses in ko\_DSS. (C) The KEGG Enrichment Analysis. This bar plot illustrates the enrichment of various KEGG pathways in the ko\_DSS and wt\_DSS groups. Each bar represents a specific pathway, with the x-axis showing the negative logarithm of the adjusted p-value ( $-\log_{10}(\text{Adjusted})$ ), indicating the significance of enrichment.

The functional analysis revealed significant metabolic reprogramming characteristics. Butyrate (a SCFA) maintains intestinal homeostasis by serving as an HDAC inhibitor, promoting Treg differentiation via epigenetic modulation of the Foxp3 locus while suppressing Th17 responses through IL-6/STAT3 inhibition (36–38). Downregulation of butyrate kinase (K01990) aligns with reduced butyrate-producing bacteria (e.g., *Faecalibacterium prausnitzii*) in IBD, exacerbating inflammation in this research. Gram-negative bacterial lipopolysaccharide (LPS) activates the TLR4-NF- $\kappa$ B-IL-23/Th17 signaling axis while simultaneously directly compromising intestinal tight junction integrity (39, 40). This pathophysiological mechanism is highly consistent with our experimental findings demonstrating significant

downregulation of occludin and claudin expression in the intestinal epithelium. These results align with clinical observations of elevated plasma LPS concentrations in IBD cases (41).

Research evidence demonstrates that the gut microbiota can significantly modulate the therapeutic efficacy of PD-1/PD-L1 inhibitors in cancer treatment (42). Specifically, in melanoma and colorectal cancer patients who are non-responders to anti-PD-1 therapy, studies have observed abnormal proliferation of Bacteroides species and significant depletion of beneficial bacteria such as *Akkermansia muciniphila* (43, 44). For the first time, our study has replicated these key findings in a PD-L1-deficient mouse model: not only confirming reduced abundance of *Akkermansia muciniphila*, but more importantly, functional predictive analysis revealed significant

upregulation of antibiotic resistance-related genes including ABC transporters (K02003/K02004),  $\beta$ -lactamase resistance genes, and multidrug efflux systems. This groundbreaking discovery suggests that deficiency in PD-L1 signaling may promote antibiotic resistance by altering the functional profile of gut microbiota—a finding with critical implications for current antibiotic-based clinical treatment strategies for IBD.

In PD-L1 knockout mice, besides an increase in pathogenic *Escherichia coli*, there is also a rise in *CAG-510* and *UBA3263* sp001689615. However, the functions and mechanisms of these two bacterial species have not yet been characterized. They may serve as biomarkers in the PD-L1 knockout mice colitis model and could be involved in the PD-L1 signaling pathway, exacerbating intestinal inflammation.

Certainly, our study has limitations regarding the relatively small sample size. However, based on the current analytical framework, we aim to further investigate the therapeutic potential of fecal microbiota transplantation using these differentially altered microbial communities for IBD treatment in subsequent research.

## Data availability statement

The datasets presented in this study can be found in online repositories. The names of the repository/repositories and accession number(s) can be found below: <https://www.ncbi.nlm.nih.gov/PRJNA1258551> <https://www.ncbi.nlm.nih.gov/PRJNA1261602>.

## Ethics statement

The animal study was approved by the Experimental Animal Center of the Eye and ENT Hospital of Fudan University. The study was conducted in accordance with the local legislation and institutional requirements.

## Author contributions

YM: Methodology, Investigation, Writing – review & editing, Formal analysis, Data curation, Visualization, Conceptualization, Writing – original draft. JS: Data curation, Visualization, Conceptualization, Formal analysis, Investigation, Methodology,

Writing – review & editing, Writing – original draft. SS: Visualization, Formal analysis, Data curation, Writing – review & editing, Methodology. LC: Resources, Project administration, Funding acquisition, Validation, Conceptualization, Writing – review & editing, Supervision.

## Funding

The author(s) declare that financial support was received for the research and/or publication of this article. This study was supported by National Natural Science Foundation of China (Grants no. 81870660) and Shanghai Science and Technology Foundation (Grants no. 22Y11910500).

## Acknowledgments

We thank Personal Biotechnology Co., Ltd. (Shanghai, China) for technical support in metagenomic sequencing and analyses.

## Conflict of interest

The authors declare that the research was conducted in the absence of any commercial or financial relationships that could be construed as a potential conflict of interest.

## Generative AI statement

The author(s) declare that Generative AI was used in the creation of this manuscript. To enhance the clarity of this manuscript

## Publisher's note

All claims expressed in this article are solely those of the authors and do not necessarily represent those of their affiliated organizations, or those of the publisher, the editors and the reviewers. Any product that may be evaluated in this article, or claim that may be made by its manufacturer, is not guaranteed or endorsed by the publisher.

## References

- Bai J, Wang Y, Li F, Wu Y, Chen J, Li M, et al. Research advancements and perspectives of inflammatory bowel disease: A comprehensive review. *Sci Prog.* (2024) 107:368504241253709. doi: 10.1177/00368504241253709
- Liao X, Liu J, Guo X, Meng R, Zhang W, Zhou J, et al. Origin and function of monocytes in inflammatory bowel disease. *J Inflammation Res.* (2024) 17:2897–914. doi: 10.2147/jir.S450801
- Vivekanandan KE, Kasimani R, Kumar PV, Meenatchisundaram S, Sundar WA. Overview of cloning in lactic acid bacteria: Expression and its application of probiotic potential in inflammatory bowel diseases. *Biotechnol Appl Biochem.* (2024) 71:881–95. doi: 10.1002/bab.2584
- Hodgkiss R, Acharjee A. Unravelling metabolite-microbiome interactions in inflammatory bowel disease through AI and interaction-based modelling. *Biochim Biophys Acta Mol Basis Dis.* (2025) 1871:167618. doi: 10.1016/j.bbdis.2024.167618
- Duan W, Zheng B, Li T, Liu R. Gut microbiota and metabolites mediate health benefits of oat and oat bran consumption in IBD mice. *Nutrients.* (2024) 16:4365. doi: 10.3390/nu16244365
- García-Gamboa R, Díaz-Torres O, Gradilla-Hernández MS, Pérez-Brocá V, Moya A, González-Avila M. Gut bacterial composition and nutritional implications in mexican and spanish individuals with inflammatory bowel disease compared to healthy controls. *Int J Mol Sci.* (2024) 25:11887. doi: 10.3390/ijms252211887

7. El-Sayed A, Kapila D, Taha RSI, El-Sayed S, Mahen MRA, Taha R, et al. The role of the gut microbiome in inflammatory bowel disease: the Middle East perspective. *J Pers Med.* (2024) 14(6):652. doi: 10.3390/jpm14060652
8. Wang A, Zhai Z, Ding Y, Wei J, Wei Z, Cao H. The oral-gut microbiome axis in inflammatory bowel disease: from inside to insight. *Front Immunol.* (2024) 15:1430001. doi: 10.3389/fimmu.2024.1430001
9. Zhao W, Li S, Li Q, Li Q, Zheng Y, Lu H. Mendelian randomization reveals predictive, preventive, and personalized insights into inflammatory bowel disease: the role of gut microbiome and circulating inflammatory proteins. *Epma J.* (2024) 15:693–709. doi: 10.1007/s13167-024-00384-2
10. Mo C, Lou X, Xue J, Shi Z, Zhao Y, Wang F, et al. The influence of Akkermansia muciniphila on intestinal barrier function. *Gut Pathog.* (2024) 16:41. doi: 10.1186/s13099-024-00635-7
11. Tang X, Chen X, Ferrari M, Walvoort MTC, de Vos P. Gut epithelial barrier function is impacted by hyperglycemia and secondary bile acids *in vitro*: possible rescuing effects of specific pectins. *Mol Nutr Food Res.* (2024) 68:e2300910. doi: 10.1002/mnfr.202300910
12. Wang X, Peng J, Cai P, Xia Y, Yi C, Shang A, et al. The emerging role of the gut microbiota and its application in inflammatory bowel disease. *BioMed Pharmacother.* (2024) 179:117302. doi: 10.1016/j.biopha.2024.117302
13. Florio M, Crudele L, Sallustio F, Moschetta A, Cariello M, Gadaleta RM. Disentangling the nutrition-microbiota liaison in inflammatory bowel disease. *Mol Aspects Med.* (2025) 102:101349. doi: 10.1016/j.mam.2025.101349
14. Fanizzi F, D'Amico F, Zanotelli Bombassaro I, Zilli A, Furfaro F, Parigi TL, et al. The role of fecal microbiota transplantation in IBD. *Microorganisms.* (2024) 12(9):1755. doi: 10.3390/microorganisms12091755
15. Parvez A, Choudhary F, Mudgal P, Khan R, Qureshi KA, Farooqi H, et al. PD-1 and PD-L1: architects of immune symphony and immunotherapy breakthroughs in cancer treatment. *Front Immunol.* (2023) 14:1296341. doi: 10.3389/fimmu.2023.1296341
16. Liu Q, Guan Y, Li S. Programmed death receptor (PD)-1/PD-ligand (L)1 in urological cancers: the “all-around warrior” in immunotherapy. *Mol Cancer.* (2024) 23:183. doi: 10.1186/s12943-024-02095-8
17. Huang YF, Zhang WM, Wei ZS, Huang H, Mo QY, Shi DL, et al. Causal relationships between gut microbiota and programmed cell death protein 1/programmed cell death-ligand 1: A bidirectional Mendelian randomization study. *Front Immunol.* (2023) 14:1136169. doi: 10.3389/fimmu.2023.1136169
18. Song S, Zhang H, Liu L, Li M, Wang X, Zeng H, et al. Probiotic DNA regulates intestinal Th2 polarization by inducing epithelial cells to produce PD-L1. *Apoptosis.* (2025) 30:239–49. doi: 10.1007/s10495-024-02043-3
19. Wu D, Hu L, Han M, Deng Y, Zhang Y, Ren G, et al. PD-1 signaling facilitates activation of lymphoid tissue inducer cells by restraining fatty acid oxidation. *Nat Metab.* (2022) 4:867–82. doi: 10.1038/s42255-022-00595-9
20. Matsushima H, Morita-Nakagawa M, Datta S, Pavicic PG Jr., Hamilton TA, Abu-Elmagd K, et al. Blockade or deficiency of PD-L1 expression in intestinal allograft accelerates graft tissue injury in mice. *Am J Transplant.* (2022) 22:955–65. doi: 10.1111/ajt.16873
21. Park SJ, Kim JH, Song MY, Sung YC, Lee SW, Park Y. PD-1 deficiency protects experimental colitis via alteration of gut microbiota. *BMB Rep.* (2017) 50:578–83. doi: 10.5483/bmbrep.2017.50.11.165
22. Fan Y, Fan Y, Liu K, Lonan P, Liao F, Huo Y, et al. Edible bird's nest ameliorates dextran sulfate sodium-induced ulcerative colitis in C57BL/6J mice by restoring the Th17/Treg cell balance. *Front Pharmacol.* (2021) 12:632602. doi: 10.3389/fphar.2021.632602
23. Martin M. Cutadapt removes adapter sequences from high-throughput sequencing reads. *EMBnet J.* (2011) 17:10–12. doi: 10.14806/ej.17.1.200
24. Chen S, Zhou Y, Chen Y, Gu J. fastp: an ultra-fast all-in-one FASTQ preprocessor. *Bioinformatics.* (2018) 34:i884–190. doi: 10.1093/bioinformatics/bty560
25. Li H. Minimap2: pairwise alignment for nucleotide sequences. *Bioinformatics.* (2018) 34:3094–100. doi: 10.1093/bioinformatics/bty191
26. Wood DE, Lu J, Langmead B. Improved metagenomic analysis with Kraken 2. *Genome Biol.* (2019) 20:257. doi: 10.1186/s13059-019-1891-0
27. Li D, Liu CM, Luo R, Sadakane K, Lam TW. MEGAHIT: an ultra-fast single-node solution for large and complex metagenomics assembly via succinct de Bruijn graph. *Bioinformatics.* (2015) 31:1674–6. doi: 10.1093/bioinformatics/btv033
28. Steinegger M, Söding J. MMseqs2 enables sensitive protein sequence searching for the analysis of massive data sets. *Nat Biotechnol.* (2017) 35:1026–8. doi: 10.1038/nbt.3988
29. Hyatt D, Chen GL, Locascio PF, Land ML, Larimer FW, Hauser LJ. Prodigal: prokaryotic gene recognition and translation initiation site identification. *BMC Bioinf.* (2010) 11:119. doi: 10.1186/1471-2105-11-119
30. Liao Y, Smyth GK, Shi W. featureCounts: an efficient general purpose program for assigning sequence reads to genomic features. *Bioinformatics.* (2014) 30:923–30. doi: 10.1093/bioinformatics/btt656
31. Segata N, Izard J, Waldron L, Gevers D, Miropolsky L, Garrett WS, et al. Metagenomic biomarker discovery and explanation. *Genome Biol.* (2011) 12:R60. doi: 10.1186/gb-2011-12-6-r60
32. Bray JR, Curtis JT. An ordination of the upland forest communities of Southern Wisconsin. *Ecol Monographs.* (1957) 27:325–49. doi: 10.2307/1942268
33. Ramette A. Multivariate analyses in microbial ecology. *FEMS Microbiol Ecol.* (2007) 62:142–60. doi: 10.1111/j.1574-6941.2007.00375.x
34. Rutigliani M, Bozzo M, Barberis A, Greppi M, Anelli E, Castellaro L, et al. Case report: A peculiar case of inflammatory colitis after SARS-CoV-2 infection. *Front Immunol.* (2022) 13:849140. doi: 10.3389/fimmu.2022.849140
35. Moreira TG, Mangani D, Cox LM, Leibowitz J, Lobo ELC, Oliveira MA, et al. PD-L1(+) and XCR1(+) dendritic cells are region-specific regulators of gut homeostasis. *Nat Commun.* (2021) 12:4907. doi: 10.1038/s41467-021-25115-3
36. Furusawa Y, Obata Y, Fukuda S, Endo TA, Nakato G, Takahashi D, et al. Commensal microbe-derived butyrate induces the differentiation of colonic regulatory T cells. *Nature.* (2013) 504:446–50. doi: 10.1038/nature12721
37. Parada Venegas D, de la Fuente MK, Landskron G, González MJ, Quera R, Dijkstra G, et al. Short chain fatty acids (SCFAs)-mediated gut epithelial and immune regulation and its relevance for inflammatory bowel diseases. *Front Immunol.* (2019) 10:277. doi: 10.3389/fimmu.2019.00277
38. Xu M, Duan X-Y, Chen Q-Y, Fan H, Z-c H, Deng S-J, et al. Effect of compound sophorae decoction on dextran sodium sulfate (DSS)-induced colitis in mice by regulating Th17/Treg cell balance. *Biomedicine Pharmacotherapy.* (2019) 109:2396–408. doi: 10.1016/j.biopha.2018.11.087
39. Chen L, Ruan G, Cheng Y, Yi A, Chen D, Wei Y. The role of Th17 cells in inflammatory bowel disease and the research progress. *Front Immunol.* (2022) 13:1055914. doi: 10.3389/fimmu.2022.1055914
40. Jia J, Zheng W, Tang S, Song S, Ai C. Scytosiphon lomentaria fucoidan ameliorates DSS-induced colitis in dietary fiber-deficient mice via modulating the gut microbiota and inhibiting the TLR4/NF- $\kappa$ B/MLCK pathway. *Int J Biol Macromolecules.* (2023) 253:127337. doi: 10.1016/j.ijbiomac.2023.127337
41. Perez-Diaz-Del-Campo N, Castelnuovo G, Ribaldone DG, Caviglia GP. Fecal and circulating biomarkers for the non-invasive assessment of intestinal permeability. *Diagnostics (Basel).* (2023) 13(11):1976. doi: 10.3390/diagnostics13111976
42. Cui JW, Li Y, Yang Y, Yang HK, Dong JM, Xiao ZH, et al. Tumor immunotherapy resistance: Revealing the mechanism of PD-1/PD-L1-mediated tumor immune escape. *BioMed Pharmacother.* (2024) 171:116203. doi: 10.1016/j.biopha.2024.116203
43. Kim Y, Kim G, Kim S, Cho B, Kim SY, Do EJ, et al. Fecal microbiota transplantation improves anti-PD-1 inhibitor efficacy in unresectable or metastatic solid cancers refractory to anti-PD-1 inhibitor. *Cell Host Microbe.* (2024) 32:1380–93.e9. doi: 10.1016/j.chom.2024.06.010
44. Huang J, Zheng X, Kang W, Hao H, Mao Y, Zhang H, et al. Metagenomic and metabolomic analyses reveal synergistic effects of fecal microbiota transplantation and anti-PD-1 therapy on treating colorectal cancer. *Front Immunol.* (2022) 13:874922. doi: 10.3389/fimmu.2022.874922